Colloids and Surfaces A 606 (2020) 125483

Contents lists available at ScienceDirect

Colloids and Surfaces A

journal homepage: www.elsevier.com/locate/colsurfa

Silica-coated magnesium ferrite nanoadsorbent for selective removal of methylene blue

Supawitch Hoijang[a], Sunanta Wangkarn[a], Pimchanok Ieamviteevanich[b], Supree Pinitsoontorn[b], Supon Ananta[c], T. Randall Lee[d], Laongnuan Srisombat[a,e,*]

[a] Department of Chemistry, Faculty of Science, Chiang Mai University, Chiang Mai, Thailand, 50200, Thailand
[b] Institute of Nanomaterials Research and Innovation for Energy (IN-RIE), Khon Kaen University, Khon Kaen, 40002, Thailand
[c] Department of Physics and Materials Science, Faculty of Science, Chiang Mai University, Chiang Mai, 50200, Thailand
[d] Department of Chemistry and the Texas Center for Superconductivity, University of Houston, Houston, TX, 77204-5003, United States
[e] Center of Excellence in Materials Science and Technology, Chiang Mai University, Chiang Mai, 50200, Thailand

GRAPHICAL ABSTRACT

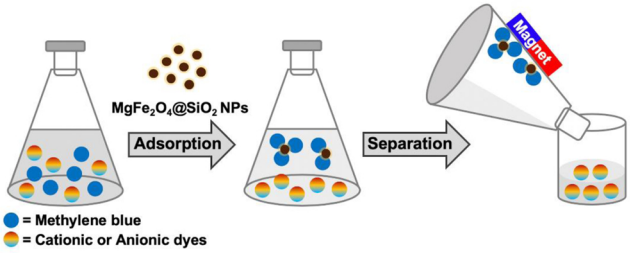

ARTICLE INFO

Keywords:
Magnesium ferrite nanoparticles
Methylene blue
Selective adsorption
Silica-coated nanoparticles
Magnetic removal

ABSTRACT

This paper demonstrates the adsorption capability of silica-coated magnesium ferrite nanoparticles ($MgFe_2O_4$@SiO_2 NPs) for the selective adsorption of methylene blue (MB). The $MgFe_2O_4$@SiO_2 NPs were generated from $MgFe_2O_4$ NPs by coating with a thin silica shell. After fully characterizing the $MgFe_2O_4$@SiO_2 NPs, selective adsorption studies were carefully investigated by using three types of representative dyes: cationic (MB, rhodamine B, and malachite green), anionic (methyl orange and Congo red), and neutral (neutral red) dyes. Efficient removal of MB by the $MgFe_2O_4$@SiO_2 adsorbents was observed for both individual and mixed dye systems, demonstrating excellent selectivity for MB. To optimize the adsorption capacity for MB removal, several parameters (*i.e.,* initial solution pH, initial dye concentration, and contact time) were carefully investigated. In all cases, the magnetoresponsive adsorbents were easily separated from the solution by using an external magnet. Regeneration of the $MgFe_2O_4$@SiO_2 NPs for MB removal was also performed to investigate the stability and reusability of the adsorbent. The recycling tests revealed that the MB removal efficiencies remained high after ten adsorption-desorption cycles. On the whole, the $MgFe_2O_4$@SiO_2 NPs were found to be efficient, selective, and reusable adsorbents for MB removal.

1. Introduction

Methylene blue (MB) is an organic dye that is used, for example, in the textile industry, for tissue staining, and in the leather tanning industry [1,2]. This essential synthetic dye, which is commonly found in natural water resources due to discharging of untreated wastes [3,4],

* Corresponding author at: Department of Chemistry, Faculty of Science, Chiang Mai University, Chiang Mai, 50200, Thailand.
E-mail address: laongnuan.sri@cmu.ac.th (L. Srisombat).

https://doi.org/10.1016/j.colsurfa.2020.125483
Received 14 June 2020; Received in revised form 17 August 2020; Accepted 17 August 2020
Available online 28 August 2020
0927-7757/

has been implicated in health issues, such as eye irritation and itchy skin as well as respiratory and digestive problems [5,6]. Therefore, it is necessary to treat dye wastewaters before their release into natural water resources.

Until now, several methods have been developed for dye removal, including adsorption [7,8], photocatalytic degradation [9–13], electrochemical degradation [14,15], Fenton reaction [16], and filtration membranes [17,18]. Among these treatment methods, adsorption is one of the most attractive for MB removal owing to ease of operation, low cost, high efficiency, no secondary pollution, and recyclable capacity [19,20]. The development of adsorbents with high adsorption capacity, selectivity, and reusability are also of interest, leading to the recent design and synthesis of several adsorbents for dye removal [21–26]. Conventional adsorbents based on activated carbon have been widely used for dye removal due to their high adsorption capacity [27,28]. However, activated carbon suffers from limitations such as high regeneration costs and especially poor selectivity [27–29].

Given these limitations, various types of a selective adsorbents for specific dye removal have been recently introduced [30–37]. For example, Fu et al. [30] synthesized polydopamine microspheres for the selective adsorption of a wide variety of dyes, including cationic, anionic and neutral dyes. The polydopamine microspheres favored the removal of the cationic dyes; methylene blue and malachite green as well as neutral red dye. Interestingly, cationic MB was completely removed from cationic/anionic dye mixtures. In separate studies, Akbari et al. [31] reported that vanadium phosphorus oxide encapsulated in TiO_2 matrixes provided high selective adsorption of MB compared with cationic rhodamine B (RhB) and anionic methyl orange (MO). In addition, the enhancement of RhB removal efficiency was found in MB/RhB mixtures due to adsorbate-adsorbate interactions. Similarly, Wang et al. [32] demonstrated that the selective adsorption of MB over RhB by porous $BiOBr/Bi_2MoO_6$ adsorbents was due to the smaller molecular size of MB. Collectively, these studies indicate that adsorbent-adsorbate charge, adsorbate-adsorbate interactions, and adsorbent pore size-adsorbate molecular dimensions play important roles for adsorption selectivity (*i.e.*, the selectivity depends not only on adsorbent-adsorbate interactions, but also adsorbate-adsorbate interactions in dye mixtures).

Another key issue for adsorbent design is separation performance, which can be considered in terms of isolation of the adsorbent from the treated solution. Generally, separation of the adsorbent after treatment can be performed by methods such as filtration and centrifugation, which can require lengthy processing times and external energy for driving the process. An alternative approach involves the use of magnetic-based dye adsorbents, which offer ease of separation by using an external magnet. For example, Huang et al. [33] used $Fe_3O_4@SiO_2$ nanoparticle-porous organic polymer composites for the selective adsorption of MB. Similarly, Song et al. [29] prepared the hyperbranched polymer/Fe_3O_4 nanoparticle composites for use as selective adsorbents for MB. Although, magnetic-based adsorbents have been extensively studied for dye adsorption, only a few studies have focused on selective dye adsorption [29].

Interestingly, magnesium ferrite nanoparticles ($MgFe_2O_4$ NPs) are alternative adsorbents for the removal of organic pollutants owing to their high specific surface area and superparamagnetic behavior [38]. In addition, $MgFe_2O_4$ NPs are non-cytotoxic, which offers both environmental safety and practical usage [39]. Nevertheless, to the best of our knowledge, studies of $MgFe_2O_4$-based nanoadsorbents for selective MB removal have not been reported. These factors led us to consider that $MgFe_2O_4$ NPs can be as potential adsorbents for MB removal. In particular, our previous studies of amine-functionalized $MgFe_2O_4$ nanoparticles ($MgFe_2O_4$–NH_2 NPs) found that these nanoparticles were effective adsorbents for anionic dyes such as Congo red (CR) and the pesticide, 2,4-dichlorophenoxyacetic acid (2,4-D) [40,41]. The anionic organic molecules were removed predominantly through electrostatic interactions between the positively charged surfaces of the $MgFe_2O_4$–NH_2 NPs and the negatively charged molecules. Thus, to remove cationic MB from wastewater, we sought to develop a new $MgFe_2O_4$-based magnetic nanoadsorbent.

Literature studies have shown that modification of the adsorbent surface can be used to enhance the adsorption capacity and selectivity of nanoparticle-based adsorbents [42,43]. For example, Dai et al. [42] and Tan et al. [44] reported that coating the surfaces of Fe_3O_4 nanoparticles with silica ($Fe_3O_4@SiO_2$ NPs) not only increased the adsorption capacity, but also the selectivity of MB compared to uncoated Fe_3O_4 nanoparticle adsorbents [44]. Given that surface modification with silica is rapid and simple [45], we sought in the present study to prepare silica-coated $MgFe_2O_4$ ($MgFe_2O_4@SiO_2$) nanoadsorbents for systematic studies of their adsorption of representative dyes (cationic, anionic, and neutral dyes). In addition, we examined the adsorption behavior of these new nanoadsorbents in the presence of several mixed dye systems, with a goal toward the selective adsorption of MB. In these studies, we examined several factors (*i.e.,* initial solution pH, initial dye concentration and contact time) in efforts to optimize the efficiency of MB removal. Adsorption isotherms of the $MgFe_2O_4@SiO_2$ NPs were estimated by using Langmuir and Freundlich models. In addition, the $MgFe_2O_4@SiO_2$ nanoadsorbents were evaluated with regard to stability and reusability.

2. Materials and methods

2.1. Materials

Magnesium ferrite nanoparticles ($MgFe_2O_4$ NPs) were prepared by employing the synthetic method reported by Nonkumwong et al. [38]. These NPs were used as cores, which were treated with 0.1 mol L^{-1} hydrochloric acid (Merck, 37 %), absolute ethanol (Merck, 99.5 % purity), ammonia solution (Merck, 25 %), and tetraethyl orthosilicate (TEOS, Sigma-Aldrich, 99.0 % purity) to affect the silica coating. Methylene blue (MB, Merck), rhodamine B (RhB, Loba chemie), malachite green (MG, Loba chemie), methyl orange (MO, KemAus), Congo red (CR, Loba chemie) and neutral red (NR, Sigma-Aldrich) were used as model organic dyes. All dyes were of analytical grade, and their chemical structures are provided in **Table S1**. All chemicals were used as received without purification.

2.2. Synthesis of silica-coated magnesium ferrite nanoparticles ($MgFe_2O_4@SiO_2$ NPs)

The procedure for coating the $MgFe_2O_4$ NPs with silica was adapted from the work reported by Xu et al. [46] with slight modification, for which the coating mechanism can be found in the literature [47,48]. The strategy used to synthesize the $MgFe_2O_4@SiO_2$ NPs is given in Scheme 1. Briefly, 200 mg of $MgFe_2O_4$ powder was added into 40 mL of 0.1 mol L^{-1} HCl and then sonicated for 10 min. After sonication, the powder was separated from the HCl solution by using an external magnet, and then 64 mL of absolute ethanol, 16 mL of deionized (DI) water, and 1 mL of ammonia solution were added. The mixed solution was again sonicated for 10 min followed by mechanical stirring at room temperature. After that, 1 mL of TEOS was slowly injected into the solution mixture and left for 12 h. The final product was washed with DI water several times and then ethanol. The powder was then dried at 45 °C overnight.

2.3. Studies of selective dye adsorption by $MgFe_2O_4@SiO_2$ NPs

To investigate the selectivity of the $MgFe_2O_4@SiO_2$ nanoadsorbents for dye removal, individual and mixtures of organic dyes were used as probe molecules. At a concentration of 5 mg L^{-1}, solutions of MB, RhB, MG, MO, CR and NR were diluted from the respective stock solutions by using DI water. Mixed dye solutions containing 5 mg L^{-1} of each dye (*i.e.*, MB/RhB, MB/MO, MB/CR, MB/NR, RhB/MO, RhB/CR, MB/RhB/MO and MB/RhB/CR) were also prepared. The dye solutions were

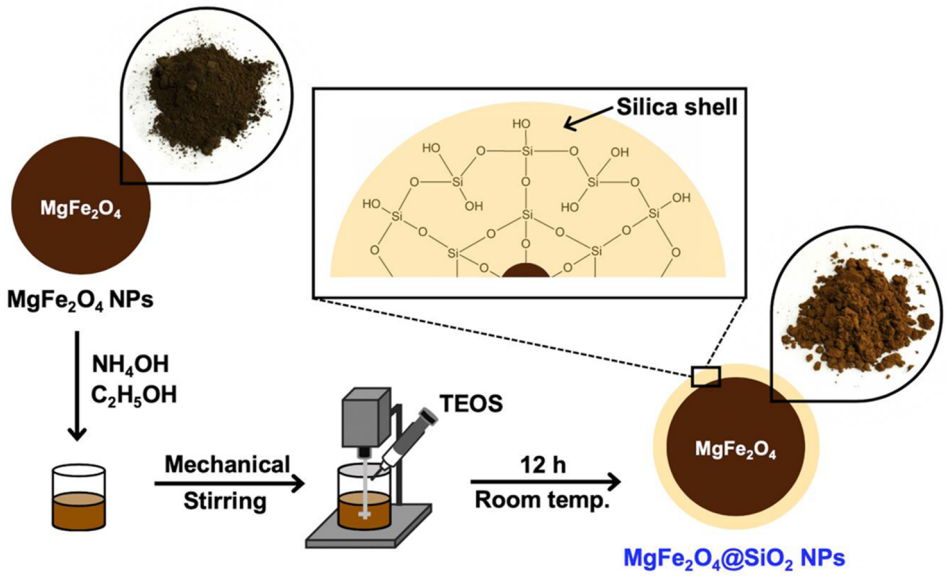

Scheme 1. Illustration of the synthesis of $MgFe_2O_4$@SiO_2 NPs. Insets: photographs before (left) and after (right) the silica-coating process.

adjusted to pH ~7, and then 15 mL aliquots of the dye solutions were treated with 42 mg of magnetic nanoadsorbents. The solutions were shaken for one hour at room temperature. After that, the nanoadsorbents were separated by using an external magnet. The amount of dye remaining after the adsorption process was measured by UV–vis spectroscopy (PG Instruments T80) at various maximum absorption wavelengths (λ_{max}), which are listed in Table S1. The selectivity of $MgFe_2O_4$@SiO_2 NPs for dye removal was determined by using the dye removal efficiencies calculated by Eq. (1):

$$\text{Removal efficiency (RE, \%)} = \frac{C_0 - C_t}{C_0} \times 100 \quad (1)$$

where C_0 and C_t are the concentrations of dye at time zero and at time t (mg L^{-1}), respectively.

2.4. Adsorption of MB by $MgFe_2O_4$@SiO_2 NPs

To obtain the maximum adsorption capacity of MB by the nanoadsorbent, several factors including initial solution pH, initial dye concentration, and contact time were optimized. All adsorption studies were performed as described in Section 2.2. First, to investigate the effect of solution pH, various 10 mg L^{-1} MB solutions at pH values of 3, 5, 7, 9, and 11 were prepared by adjusting with 0.1 mol L^{-1} sodium hydroxide and hydrochloric acid. Second, different concentrations of MB solution were used to study the influence of initial dye concentration (*i.e.*, 100 mg L^{-1} of MB solution was reduced to 10, 15, and 20 mg L^{-1} by dilution with DI water). Finally, to determine the rate of MB uptake by the nanoadsorbent, the adsorption time was carefully controlled at 1, 3, 5, and 10 min.

To study the adsorption isotherms, MB concentrations ranging from 5 to 200 mg L^{-1} were used at pH 9. The quantity of MB adsorbed on the $MgFe_2O_4$@SiO_2 NPs at time t (q_t) was calculated by using Eq. (2):

$$q_t\ (mgg^{-1}) = \frac{(C_0 - C_t)V}{m} \quad (2)$$

where V and m are the volume of MB solution and the dry weight of the adsorbent, respectively.

2.5. Regeneration and reusability

To explore the recycling capacity of the nanoadsorbent, adsorption-desorption studies were performed. First, 42 mg of freshly prepared $MgFe_2O_4$@SiO_2 NPs were mixed with 15 mL of MB solution (10 mg L^{-1}) at pH 9. The mixture was shaken for one hour at room temperature. After separation of the $MgFe_2O_4$@SiO_2 NPs from the solution, the remaining of MB in the solution was evaluated by UV–vis spectroscopy. The used nanoadsorbent was kept in an oven at 80 °C overnight. The desorption process was started by adding the used nanoadsorbent to 15 mL of absolute ethanol, an eluting agent, and then the mixture was shaken at room temperature for one hour. Afterward, the used nanoadsorbent was washed by 15 mL of 0.1 mol L^{-1} sodium hydroxide, followed by two washings with DI water. The nanoadsorbent was then dried in an oven 80 °C for six hours and used for next adsorption process. This adsorption-desorption process was counted as the first cycle. In this work, ten adsorption-desorption cycles were conducted for each assay.

2.6. Characterization

The phase of the magnetic $MgFe_2O_4$ nanoparticles after silica coating was identified by X-ray diffraction (XRD, Rigaku SmartLab) by using Cu Kα radiation (λ = 1.5406 Å) with 0.02° scan steps at 2θ ranging from 15° to 85°. Surface modification of the as-synthesized powder was investigated by Fourier-transform infrared spectroscopy (FT-IR, Bruker TENSOR 27) at wavenumbers from 400 to 4000 cm^{-1} by using the KBr pellet method. The morphology was examined by transmission electron microscopy (TEM, JEOL JEM-2010) with 200 kV of accelerating voltage and field emission scanning electron microscopy (FE-SEM, JEOL JSM-6635 F). The energy spectra of elements in materials were also recorded by an energy dispersive X-ray spectroscopy (EDS) detector connected with the FE-SEM. Zeta potential measurements were performed at room temperature on a Zetasizer Nano ZS (Brookhaven ZetaPALS) at pH values ranging from 3 to 12 adjusted by 0.1 mol L^{-1} hydrochloric acid and 0.1 mol L^{-1} sodium hydroxide. The powder was dispersed by using 0.1 mg mL^{-1} concentration and then adjusting the ionic strength to 1 × 10^{-3} mol L^{-1} by using sodium chloride. The magnetic properties of the samples were measured by a vibrating magnetometer (VSM, Quantum Design Versalab) using an applied field range of ± 10 kOe at room temperature. The specific surface area, pore volume, and pore size of the as-synthesized $MgFe_2O_4$@SiO_2 adsorbent were determined by using two well-known methods: Brunauer–Emmett–Teller (BET) and Barrett–Joyner–Halenda (BJH) *via* N_2 adsorption-desorption isotherms on a surface area and pore size

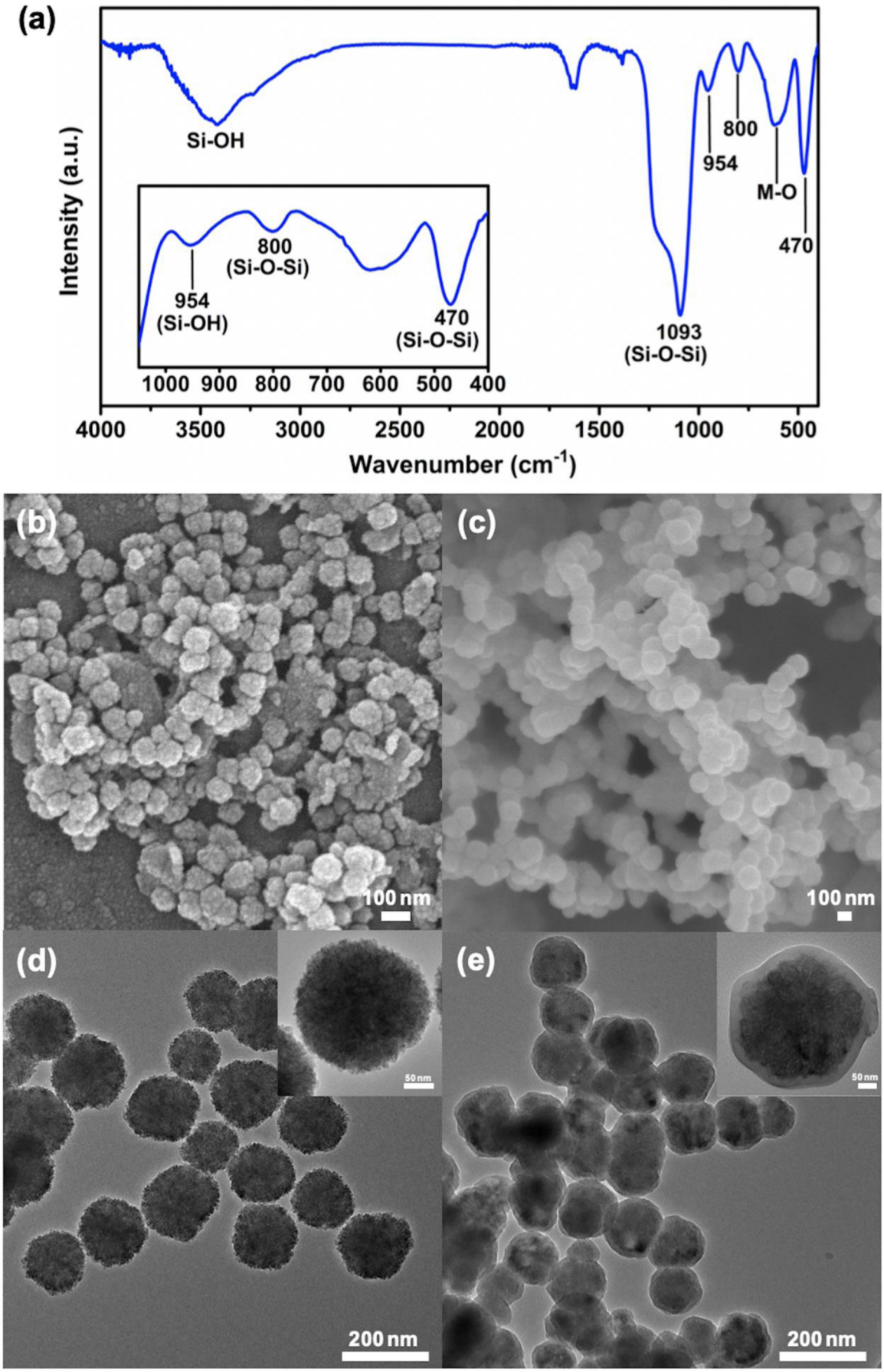

Fig. 1. (a) FT-IR spectrum of $MgFe_2O_4$@SiO_2 NPs. (b-c) FE-SEM and (d-e) TEM images of (left) $MgFe_2O_4$ NPs and (right) $MgFe_2O_4$@SiO_2 NPs.

analyzer (Autosorb 1 MP, Quantachrome). Before analysis, the sample was dehydrated at 120 °C.

3. Results and discussion

3.1. Characterization of $MgFe_2O_4$@SiO_2 NPs

To identify the phase of the silica-coated $MgFe_2O_4$ NPs, an XRD pattern was recorded as provided in **Fig. S1**. The pattern shows an excellent match with JCPDS file no. 88-1935, indicating that the pure phase of cubic spinel $MgFe_2O_4$ was obtained without any impurities after surface modification by silica. FT-IR was used to confirm the presence of silica on the as-synthesized nanoparticles. The FT-IR spectrum (Fig. 1a) shows a band at ~954 cm^{-1} and a broad band at ~3400 cm^{-1}, consistent with the bending mode of silanol (Si–OH) groups and hydroxyl (–OH) stretching of Si−OH, respectively [49]. The characteristic bands at ~1093, ~800, and ~470 cm^{-1} are assigned to the stretching and bending vibrations of siloxane groups (Si–O–Si) [43,49,50]. This finding shows the successful functionalization of $MgFe_2O_4$ NPs by silica in this study. In addition, the vibration of metal oxide (Fe–O and Mg–O) can be also observed at ~500−750 cm^{-1} [40,43].

The morphologies of pristine $MgFe_2O_4$ NPs and $MgFe_2O_4$@SiO_2 NPs were explored by FE-SEM as shown in Fig. 1**b-c**. The surfaces of $MgFe_2O_4$ NPs are quite rough due to aggregation of primary particles, while the $MgFe_2O_4$@SiO_2 surfaces are smoother due to the coverage of SiO_2 on the surface of $MgFe_2O_4$ NPs. In addition, the EDS signal of silicon (Si) was detected only in the $MgFe_2O_4$@SiO_2 NPs (see **Fig. S2**). This observation is consistent with the FT-IR results, which both indicate coating of the $MgFe_2O_4$ surface by SiO_2. Apart from the FE-SEM and EDS results, TEM was also used to provide important evidence to confirm the successful surface coating of $MgFe_2O_4$ NPs by SiO_2. Fig. 1**d-e** show the 2D images of as-obtained samples before and after surface modification by silica. The images show that the $MgFe_2O_4$@SiO_2 nanoparticles are composed of two layers (inset of Fig. 1e). The inner layer is attributed to the $MgFe_2O_4$ core with diameter of ~100 nm, while the outer layer is attributed to silica shell with a thickness of ~30 nm. Additionally, the images seem to indicate that the modification process gives both mono- and poly-clusters encapsulated by silica. To investigate the specific surface area and porosity of the $MgFe_2O_4$@SiO_2 adsorbent, BET and BJH methods were used to calculate those values *via* N_2 adsorption-desorption isotherms as given in **Fig. S3**. The estimated BET specific surface area (S_{BET}), specific pore volume, and average pore radius of the as-prepared $MgFe_2O_4$@SiO_2 NPs are 20 m^2 g^{-1}, 0.1 cm^3 g^{-1}, and 6 nm, respectively. After coating with silica, the values of S_{BET} and specific pore volume of $MgFe_2O_4$@SiO_2 significantly decreased in comparison to the uncoated $MgFe_2O_4$ NPs [38]. This finding might be due to aggregation of adsorbent after coating with silica as shown in the SEM and TEM images in Fig. 1**c** and **1e**, respectively.

To further confirm the surface modification of $MgFe_2O_4$ NPs by silica, the surface charge properties of the $MgFe_2O_4$@SiO_2 NPs were also investigated by zeta potential measurement as given in Fig. 2. The pH at the point of zero charge (pH_{PZC}) for the $MgFe_2O_4$@SiO_2 NPs obtained from the zeta potential curve is ~4.9, indicating the successful surface modification by silica of $MgFe_2O_4$ NPs; notably, pH_{PZC} of the uncoated $MgFe_2O_4$ NPs is ~8.4 as previously reported by our group [38,40]. According to the several characterization techniques utilized (XRD, FT-IR, FE-SEM, EDS, TEM, and zeta potential measurements), we conclude that the $MgFe_2O_4$@SiO_2 NPs were successfully prepared in this work. According to the literature, the composite materials can be used in several applications (*e.g.,* electronic devices [51], optical devices [52], and water pollutant treatments). In this study, we focus on the application of the synthesized $MgFe_2O_4$@SiO_2 NPs as selective adsorbents for water pollutant treatment.

To explore the magnetic properties of the magnetic nanoparticles,

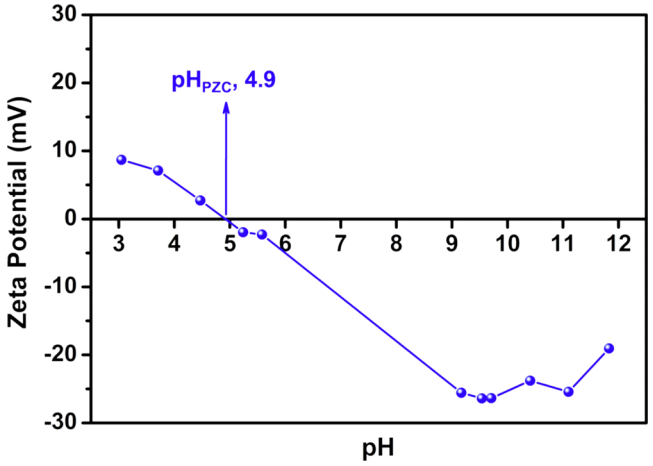

Fig. 2. Zeta potential plot of $MgFe_2O_4$@SiO_2 NPs as a function of solution pH measured at room temperature.

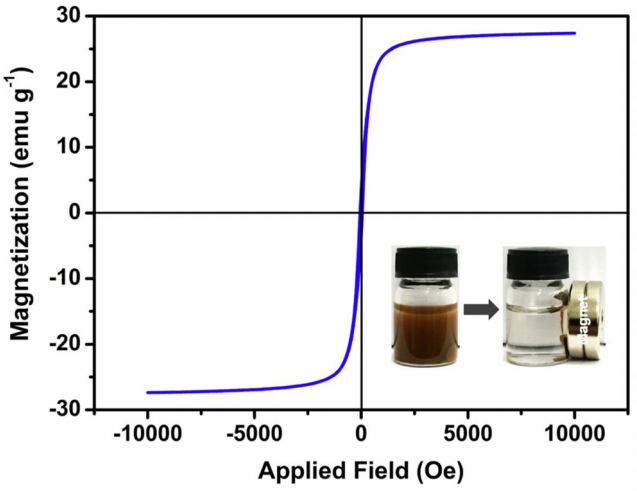

Fig. 3. Magnetization curve of $MgFe_2O_4$@SiO_2 NPs (inset: digital image of adsorbent separation from the solution using an external magnet).

we recorded magnetic hysteresis loops by tailoring the magnetic field as presented in Fig. 3. The saturation magnetization (M_s) value of the as-obtained $MgFe_2O_4$@SiO_2 NPs (~27 emu g^{-1}) is reduced compared with the M_s of the pristine $MgFe_2O_4$ NPs (~37 emu g^{-1}) [40] due to presence of the silica coating. However, the $MgFe_2O_4$@SiO_2 nanoadsorbent still exhibits excellent magnetic properties since this adsorbent can be easily separated from solution by using an external magnet within three minutes (demonstrated in an inset of Fig. 3), which is similar to that of the uncoated $MgFe_2O_4$ NPs reported in our previous studies [38,40]. This result indicates that although coating of SiO_2 on the surface of $MgFe_2O_4$ causes a reduction in the M_s value, excellent magnetic properties are still retained.

3.2. Studies of selective dye adsorption by $MgFe_2O_4$@SiO_2 NPs

The $MgFe_2O_4$@SiO_2 nanoparticles were used as adsorbents for the removal of six organic dyes: cationic dyes (MB, RhB, and MG), anionic dyes (MO and CR), and neutral dye (NR). The digital photos of each dye solution before and after the adsorption process are shown in Fig. 4**a**. The blue color of the MB solution turned to nearly colorless after the adsorption process. Likewise, the solution colors of MG and NR significantly reduced after exposure to the $MgFe_2O_4$@SiO_2 NPs. In contrast, it seems that the solution colors of RhB, MO, and CR before and after the adsorption process showed no significant differences. Apart

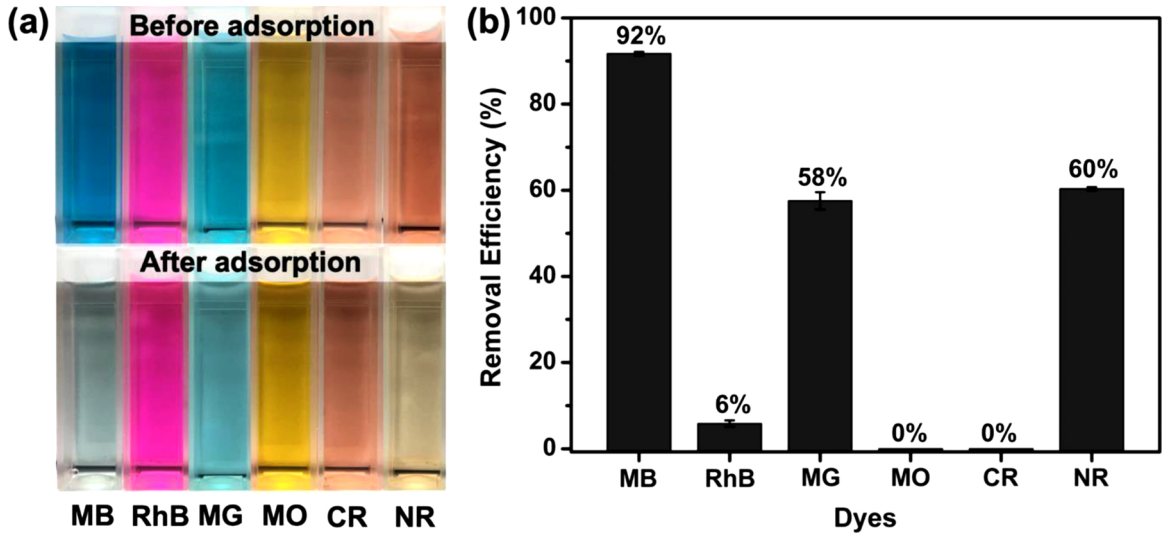

Fig. 4. (a) digital photos of appeared color of solutions before and after treatments and (b) removal efficiencies of dyes by $MgFe_2O_4@SiO_2$ NPs. Initial concentration of dye is 5 mg L^{-1} at pH ~7. Adsorbent dose is 2.8 g L^{-1}.

from the observation of physical appearance of solution, the successful adsorption of dyes can be confirmed by the absorbance signals detected by UV–vis spectroscopy as shown in **Fig. S4**. The absorbance signals of MB, MG, NR decreased substantially, indicating again that the MB, MG, and NR dyes were removed by the $MgFe_2O_4@SiO_2$ NPs. In addition, the absorption band for RhB dropped slightly, suggesting a low adsorption efficiency. Notably, there were no noticeable reductions in the absorbance signals for MO and CR after the treatment process, indicating little or no adsorption for the anionic dyes by the $MgFe_2O_4@SiO_2$ nanoadsorbent. From the UV–vis spectra, the removal efficiencies of dyes can be calculated by using Eq. (1) and are provided in Fig. 4**b**. The removal efficiencies of MB, RhB, MG, and NR by the $MgFe_2O_4@SiO_2$ NPs are ~92 %, ~6 %, ~58 %, and ~60 %, respectively.

Generally, several factors can affect dye adsorption such as the adsorption conditions (*e.g.,* initial solution pH, initial dye concentration, and contact time) as well as the adsorbent type [43,50]. Among these factors, the surface charge of the adsorbent, which varies with adsorbent type, is one of the most important factors. The pH at the point of zero charge (pH_{PZC}) of the adsorbent is used here to classify the surface charge. The adsorbent surface becomes positively charged when $pH < pH_{PZC}$ and negatively charged when $pH > pH_{PZC}$ [30]. In our studies, the initial pH of the solution was carefully kept at ~7, which is higher than the pH_{PZC} of $MgFe_2O_4@SiO_2$ NPs, ~4.9. Therefore, the surface of proposed adsorbent should be negatively charged, which is consistent with the capacity of the nanoadsorbent to remove cationic dyes such as MB and MG *via* electrostatic interactions. Generally, NR is categorized as a neutral dye [30,53]; however, it can exist in either neutral or cationic form, which depends on pH of media solution [54]. In this study, NR presented in cationic form because the pH of solution was ~7, which explains why NR could be adsorbed by $MgFe_2O_4@SiO_2$ NPs similar to MB and MG cationic dyes. On the other hand, MO and CR could not be removed by $MgFe_2O_4@SiO_2$ NPs owing to repulsion of negatively charged of MO and CR with the negatively charged surface of the nanoadsorbent. These results lead us to conclude that the $MgFe_2O_4@SiO_2$ adsorbent is suitable for removing cationic dyes.

Considering the cationic dyes, the affinity of adsorption onto the $MgFe_2O_4@SiO_2$ NPs follow this order: MB > MG ~ NR > > RhB. The differences here can perhaps be due to the steric bulk of the dyes. According to the estimated molecular sizes of the dyes (chemical structures listed in **Table S1**), MB (1.26 × 0.77 × 0.65 nm) [55], RhB (1.59 × 1.18 × 0.56 nm) [55], and MG (1.38 × 0.99 × 0.42 nm) [56], the steric bulk, which is considered as the length along the *x*-axis, follows the order MB < MG < RhB. In short, the smaller molecules are adsorbed most efficiently.

Additionally, Trujillo et al. [57] recently reported that the interaction of hydrophilic adsorbent surfaces with MB and MG molecules involves multiple supramolecular interactions (*e.g.,* O–H—N and cation–π) determined by the number of donor/acceptor sites on the dye molecule [57]. MB has three donor/acceptor sites (N atoms in its structure), which is more than that of MG, an observation that is consistent with the stronger affinity of MB toward the $MgFe_2O_4@SiO_2$ NPs studied here. Previously, Fu et al. [30] evaluated polydopamine microspheres for the selective adsorption of the individual dyes MB, MG, and NR. The removal efficiencies of those dyes were found to be ~86 %, ~92 %, and ~94 %, respectively, and the adsorbent could remove all dyes when mixed together due to such high removal efficiencies. On the other hand, in the same situation, $MgFe_2O_4@SiO_2$ NPs remove MB selectively in the presence of MG and NR (see below) since the removal efficiencies of MB, MG, and NR by $MgFe_2O_4@SiO_2$ NPs are ~92 %, ~58 %, and ~60 %, respectively. Therefore, these studies illustrate the excellent selective adsorption of MB by the $MgFe_2O_4@SiO_2$ NPs.

To confirm the selectivity of cationic dye adsorption by the $MgFe_2O_4@SiO_2$ NPs, we examined the adsorption behaviors of three sets of mixed dyes (*i.e.*, cationic/anionic, cationic/cationic, and three mixed dye systems). The cationic/anionic dye mixtures: MB/MO, MB/CR and RhB/MO were used as the first set of adsorbates (see Fig. 5). The color of the MB/MO mixture turned from green to yellow after adsorption, suggesting that MB was preferably adsorbed by the $MgFe_2O_4@SiO_2$ NPs. Similarly, the ocean color of the MB/CR mixture also faded after the treatment process. Also, the absorption bands of MB in the MB/MO and MB/CR mixtures dramatically decreased, consistent with the solution color changes. These results show that almost all of the MB in the mixtures was removed by the nanoadsorbent.

Interestingly, the UV–vis spectrum of MB/CR in Fig. 5**b** before adsorption showed remarkable reduction of the MB absorbance signal and a blue shifting of the λ_{max} of CR when compared with those obtained from individual MB and CR solutions at the same concentration. These observations suggest that the CR molecule interacts with the MB molecule in solution. Yang et al. [58] reported that CR molecules can bind one by one with MB molecules *via* hydrogen bonding and van der Waals interactions as confirmed by fluorescence spectroscopy. Yang's study also reported that the presence of MB in dye mixture led to an increase of the CR removal efficiency by the $MnFe_2O_4$ adsorbent. They proposed that not only CR molecules can be adsorbed directly by the adsorbent, but also trapped with MB molecules [58]. In contrast, having MB in mixed dye systems did not enhance the removal efficiency of CR by our

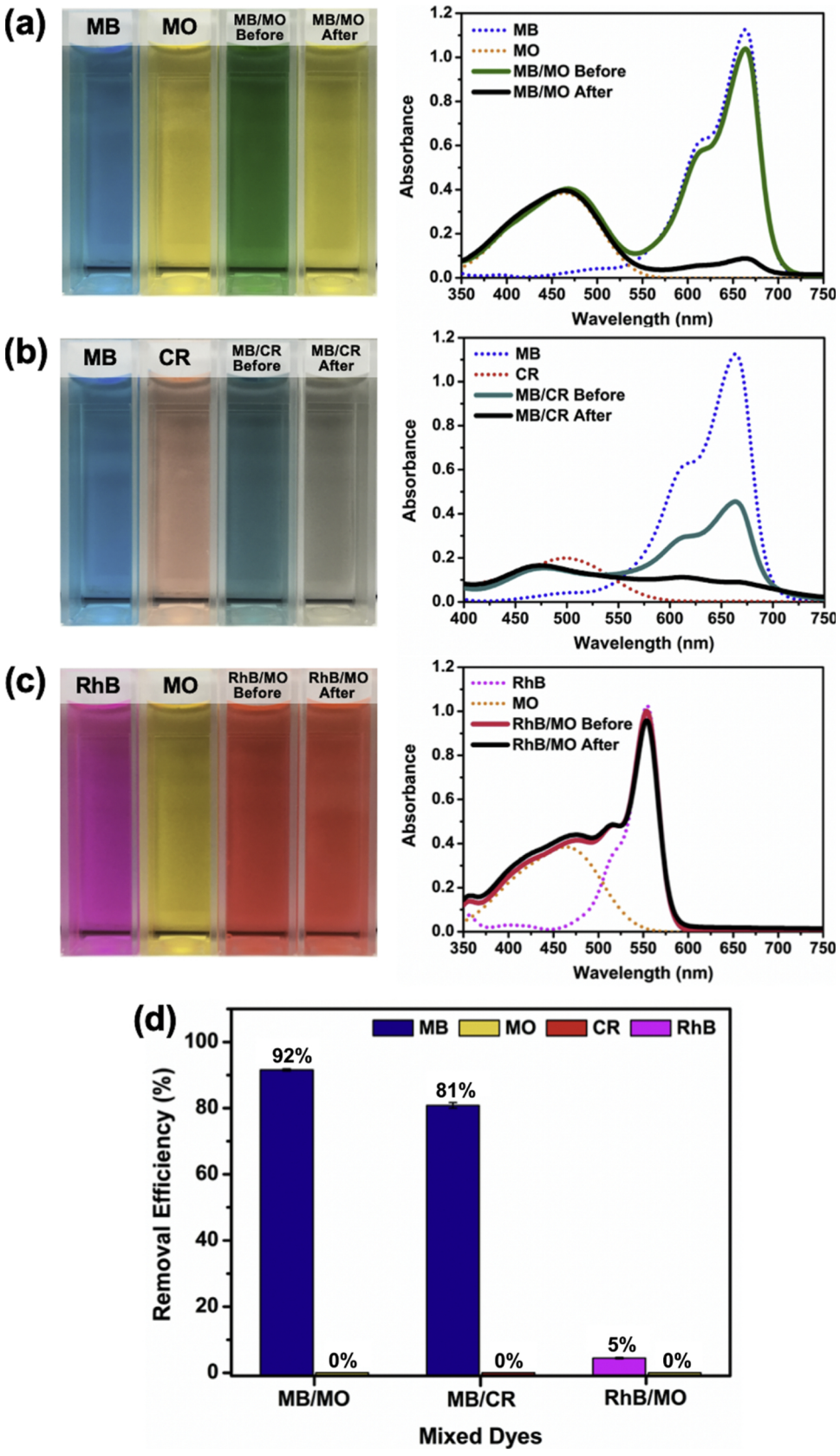

Fig. 5. (left) Digital photos and (right) UV–vis spectra of the mixed cationic/anionic dye solutions: (a) MB/MO, (b) MB/CR and (c) RhB/MO before and after adsorption by $MgFe_2O_4@SiO_2$ NPs. (d) The relative removal efficiencies of dye in cationic/anionic mixed dye solutions by $MgFe_2O_4@SiO_2$ NPs.

$MgFe_2O_4$@SiO_2 nanoadsorbent. Furthermore, the MB absorbance signal was significantly reduced upon increasing the initial concentration of CR as shown in **Fig. S5**. Considering the RhB/MO mixture, the solution color showed no noticeable changes. However, the absorbance signal of RhB after the treatment process slightly decreased, while the signal of MO did not decrease. A remarkable decrease in the solution colors of MB in MB/MO and MB/CR mixtures was accompanied by significant decrease of the MB absorption band in the mixed dye solutions. These results strongly indicate that high removal efficiency of MB by $MgFe_2O_4$@SiO_2 NPs; specifically, the removal efficiencies (see Fig. 5d) of MB in the MB/MO and MB/CR mixtures are ~92 % and ~81 %, respectively, while only ~5 % of RhB was removed from the RhB/MO mixture. Furthermore, there was no adsorption of MO in the MB/MO and RhB/MO mixtures by $MgFe_2O_4$@SiO_2 NPs (0 % removal efficiency) confirmed by the appearance the MO color in the mixtures and no obvious change of the MO absorption band after the treatment process. According to the results, we conclude that the $MgFe_2O_4$@SiO_2 NPs are efficient agents for MB removal (> 80 %) in the presence of anionic dyes.

We evaluated a second set of mixed dyes containing cationic/cationic dye mixtures: MB/RhB, MB/NR, RhB/MG, RhB/NR, and MG/NR (see Fig. 6). The blue-violet color of MB/RhB changed to the fuchsia color of RhB, indicating that MB was largely removed. The decrease of the MB absorption band indicated ~91 % of MB removal efficiency, which is close to the removal efficiency of individual MB, ~92 %. The result shows that the $MgFe_2O_4$@SiO_2 NPs favor the adsorption of MB rather than RhB, which can perhaps be attributed to the greater steric bulk of the RhB molecule [31,35]. In addition, deprotonation of the carboxyl group ($–COO^-$), which occurs at pH > 3, reduces the overall positive charge of the RhB molecule [59], leading to weak adsorption of RhB by the $MgFe_2O_4$@SiO_2 nanoadsorbent.

The mixture of cationic/cationic dyes, MB/NR, was used as a model of almost similar chemical structure and molecular size of adsorbates. The absorption bands of MB and NR noticeably declined in mixture after the adsorption process (Fig. 6b), indicating that the MB and NR molecules were captured by the nanoadsorbent. The removal efficiencies of MB and NR were ~93 % and ~74 %, respectively (Fig. 6f). Compared to that of the individual NR dye, the NR adsorption efficiency obtained from the mixed MB/NR solution increased slightly. The slight increase of NR adsorption efficiency might be due to the interaction between the NR and MB molecules *via* hydrogen bonding and π–π interactions [58]. These MB–NR interactions were expected based on the results above of the MB/CR mixtures.

To confirm the weak adsorption of RhB by $MgFe_2O_4$@SiO_2 NPs, we evaluated dye mixtures of RhB/MG and RhB/NR. Fig. 6**c-d** show that the solution colors of RhB/MG and RhB/NR changed to the color tone of the RhB solution after adding the $MgFe_2O_4$@SiO_2 NPs to the mixed solution. The absorption bands of MG and NR considerably diminished, contrary to the absorption band of RhB. Fig. 6**f** shows that the RhB removal efficiencies are ~8 % and ~17 % for RhB/MG and RhB/NR, respectively. However, MG and NR in the RhB-based mixtures were largely removed, providing adsorption efficiencies of ~65 % and ~50 % for MG and NR, respectively. For RhB, the removal efficiencies of RhB in mixtures of MB/RhB (~15 %) and RhB/NR (~17 %) increased in comparison with the adsorption efficiency of individual RhB (~6 %). This phenomena might be affected by the attractive interactions of between the RhB molecules and the MB or NR molecules through van der Waals interactions, leading to a greater amount of RhB adsorbed in the presence of MG or NR dyes [31]. Akbari et al. [31] found that the removal efficiency of RhB in MB/RhB mixtures by VPO@TiO_2 adsorbents significantly increased from ~8 % to ~78 % in comparison with that found with RhB alone. Regarding the adsorption of the cationic MG/NR dye mixture (Fig. 6e), the solution color faded, and the absorption bands of MG and NR were also diminished. The removal efficiencies of MG and NR in the MG/NR mixture (Fig. 6**f**) were ~65 % and ~53 %, respectively, which were almost equal to the removal efficiencies obtained from the individual dye solutions.

The adsorption behaviors of the third set of mixed dyes MB/RhB/MO and MB/RhB/NR are illustrated in Fig. 7. Considering the MB/RhB/MO mixture, the absorption band of MB dramatically decreased, indicating high removal efficiency for MB, ~89 %. And in the MB/RhB/NR mixture, a high adsorption efficiency of ~92 % was still obtained for MB. However, ~69 % of NR in the MB/RhB/NR mixture was removed, which is consistent with the adsorption behavior of NR described above. These collective studies lead us to conclude that the $MgFe_2O_4$@SiO_2 nanoadsorbent is selective to cationic dyes, especially MB since high removal efficiencies (> 80 %) were observed in all systems studied. We note that the MB molecule has lesser steric bulk and also a greater number of donor/acceptor sites than the other cationic dyes studied [55–57]. These factors might rationalize why the MB dye interacts more strongly with the $MgFe_2O_4$@SiO_2 nanoadsorbent than do the other dyes. Therefore, we chose to investigate the MB dye further *via* studies of adsorption capacities (q_m), isotherms, and kinetics. Moreover, we also investigated the influence of adsorption time, initial solution pH, and initial dye concentration.

3.3. Factors affecting to the adsorption of MB by $MgFe_2O_4$@SiO_2 NPs

The influence of initial solution pH. Generally, the adsorption efficiency derived from electrostatic interactions is significantly affected by the initial solution pH [29,57]. Fig. 8**a** shows the effect of pH on the removal of MB by the $MgFe_2O_4$@SiO_2 nanoadsorbent. At pH 3, the lowest MB removal efficiency, ~8 %, was observed due to electrostatic repulsion between the positively charged MB and the positively charged nanoadsorbent. Since the pH of the MB solution was lower than the pH_{PZC} of the $MgFe_2O_4$@SiO_2 NPs (~4.9, Fig. 2), the surface of the nanoadsorbent was positively charged. A noticeable increase of adsorption efficiency from ~8 % to ~73 % was observed upon tuning the solution pH from 3 to 5. At pH 5, the surface of the nanoadsorbent becomes slightly negatively charged, which leads to the increased binding between cationic MB and the nanoadsorbent. Furthermore, when the solution pH was increased from 5 to 11 (thereby increasing the negative charges on the nanoadsorbent), the removal efficiency for MB gradually increased from ~73 % to ~97 %.

These studies demonstrate that the variations in adsorption efficiency were influenced by pH, and that electrostatic interactions between the adsorbent and the dye molecules are of paramount importance. In particular, we believed that the adsorption of MB mainly occurred *via* electrostatic attraction between cationic MB and the negatively charged hydroxyl groups on the adsorbent surface. Although the highest removal efficiency for MB (~97 %) was obtained at pH ~11, strongly alkaline conditions should be avoided for practical applications due to environmental concerns. Therefore, we chose to keep the initial pH of the MB solution at ~9 in further studies.

The influence of initial MB concentration. Fig. 8**b** shows the removal efficiency of MB by $MgFe_2O_4$@SiO_2 NPs at various initial concentrations of MB solution. The removal efficiency of MB slightly dropped from ~85 % to ~60 % with an increase in the initial MB concentration from 10 to 20 mg L^{-1}. The nanoadsorbent dosage was kept constant along with the limited active sites available on the surface of the nanoadsorbent, whereas the amount of MB molecules was increased. This suggests that a large number of MB molecules cannot be captured by the restricted number of active sites (*i.e.*, the nanoadsorbent became saturated), leading to the observed reduction in MB removal efficiency. Therefore, the maximum removal efficiency for MB (~85 %) was performed by using 10 mg L^{-1} of MB concentration at pH ~9.

The influence of contact time. To determine the maximum adsorption capacity of MB by $MgFe_2O_4$@SiO_2 NPs, the adsorption time was also optimized as shown in Fig. 8**c**. The adsorption rate of MB rapidly rose to ~85 % within a minute and then levelled off at ~86 % after five minutes. In addition, preliminary results (not shown) indicate no significant increase in MB removal efficiency after ten minutes probably

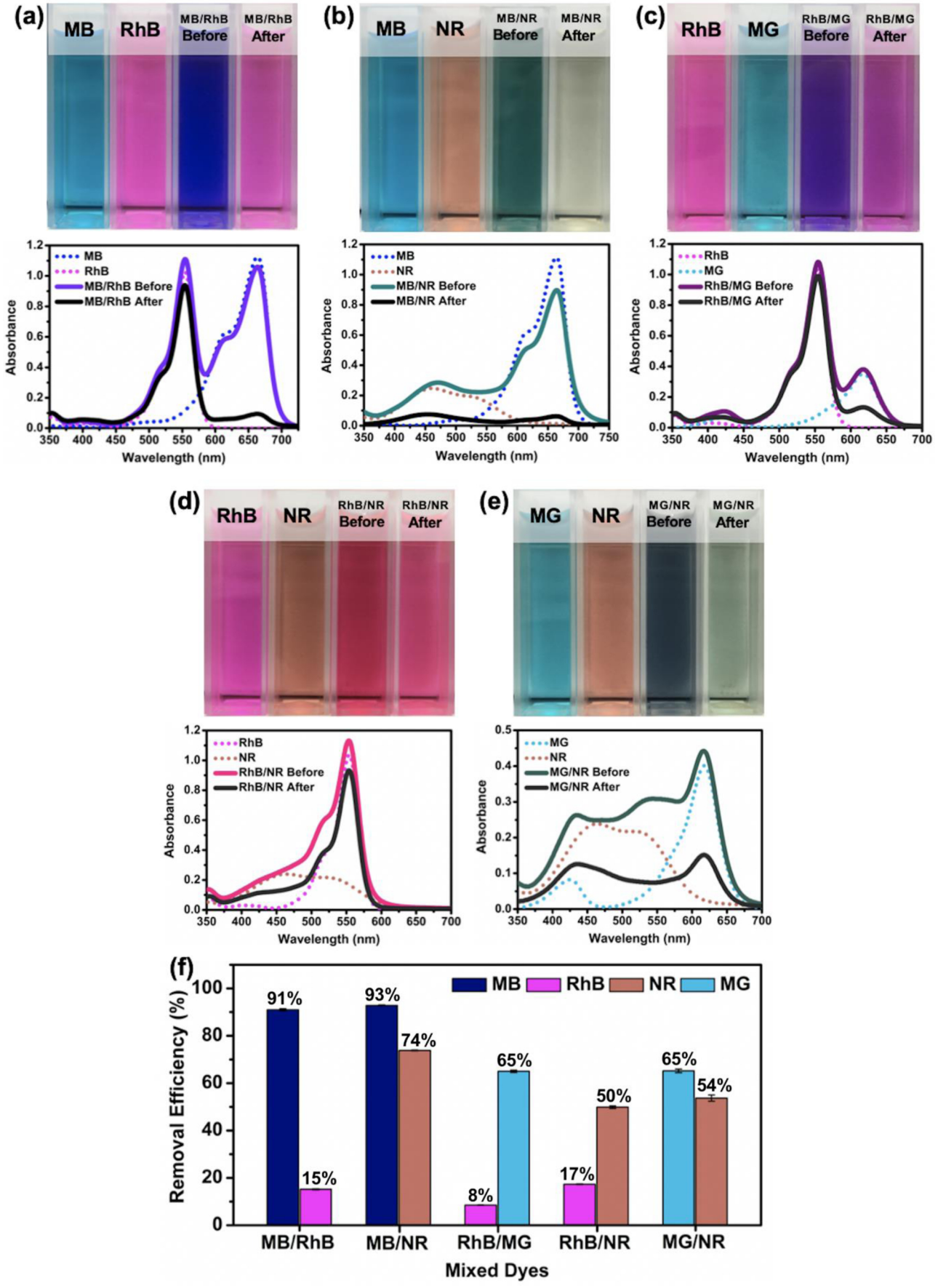

Fig. 6. (top) Digital photos and (bottom) UV–vis spectra of mixed cationic/cationic dye solutions: (a) MB/RhB, (b) MB/NR, (c) RhB/MG, (d) RhB/NR and (e) MG/NR before and after adsorption by $MgFe_2O_4@SiO_2$ NPs. (d) The relative removal efficiencies of dye in cationic/cationic mixed dye solutions by $MgFe_2O_4@SiO_2$ NPs.

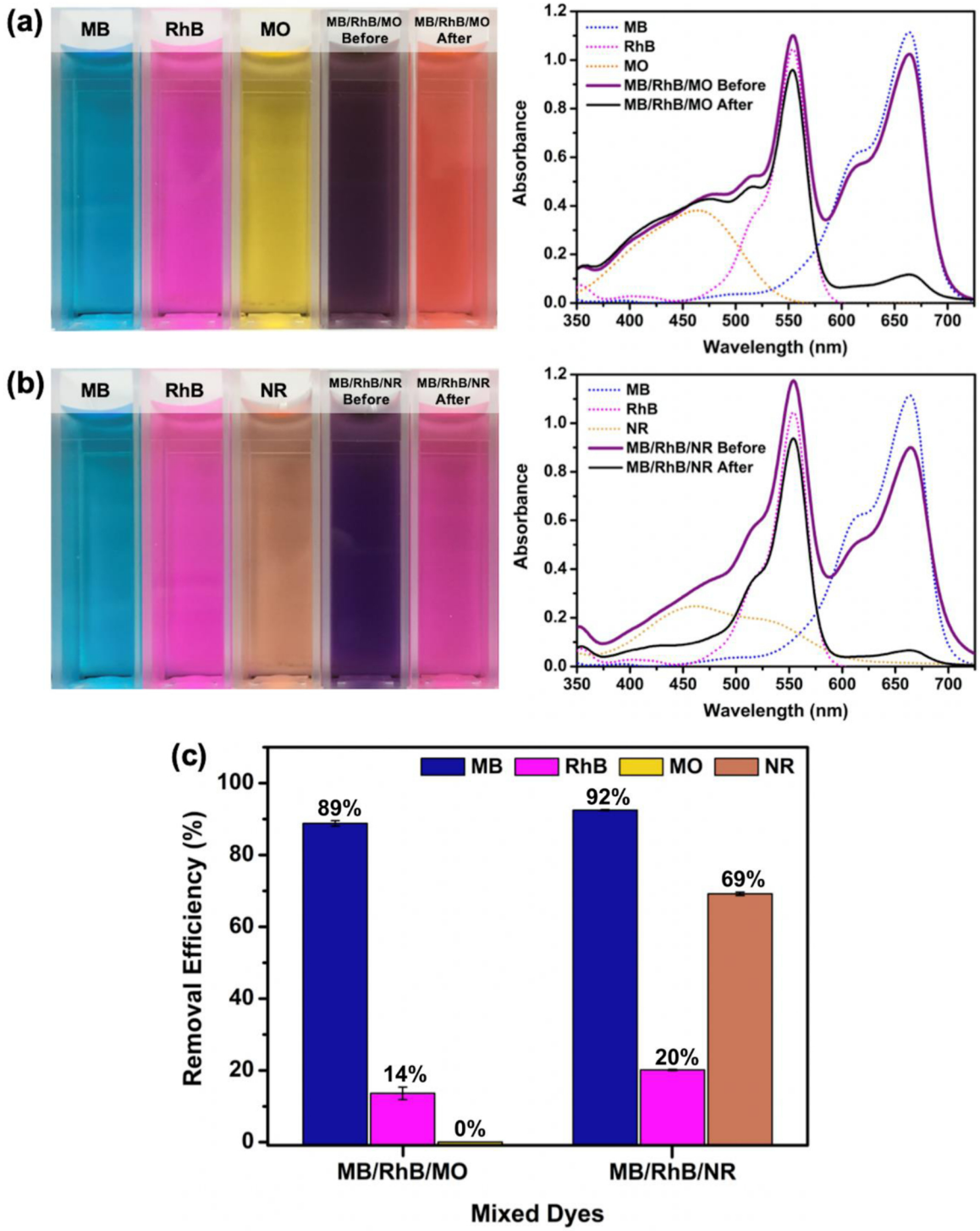

Fig. 7. (left) Digital photos and (right) UV–vis spectra of three mixed dye solutions: (a) MB/RhB/MO and (b) MB/RhB /NR before and after adsorption by $MgFe_2O_4$@SiO_2 NPs. (c) The relative removal efficiencies of dye in three mixed dye solutions by $MgFe_2O_4$@SiO_2 NPs.

due to saturation of the active sites on the nanoadsorbent surface. These findings indicate a short equilibration time for the adsorption of MB by the $MgFe_2O_4$@SiO_2 NPs. We studied the MB adsorption kinetics of the $MgFe_2O_4$@SiO_2 NPs by using 10 mg L^{-1} of MB concentration at pH ~9. **Fig S6** shows that the adsorption follows pseudo-second-order kinetics with R^2 0.999, which is consistent with a model in which the adsorption of MB by $MgFe_2O_4$@SiO_2 NPs was occurs through a chemisorption process. Generally, rapid adsorption is a highly important consideration for adsorbent selection [60]. Consequently, our data show that the $MgFe_2O_4$@SiO_2 nanoadsorbent can plausibly serve as an alternative adsorbent for decontamination of MB in wastewater, similar to competing adsorbents found in the literature [35,44].

3.4. Adsorption isotherms

In many cases, insight can be gained regarding the interactions between adsorbates and adsorbents by studying adsorption isotherms. Several models of adsorption isotherms, especially Langmuir and Freundlich isotherms, are widely used to rationalize adsorption behaviors [61]. The Langmuir adsorption isotherm is based on several

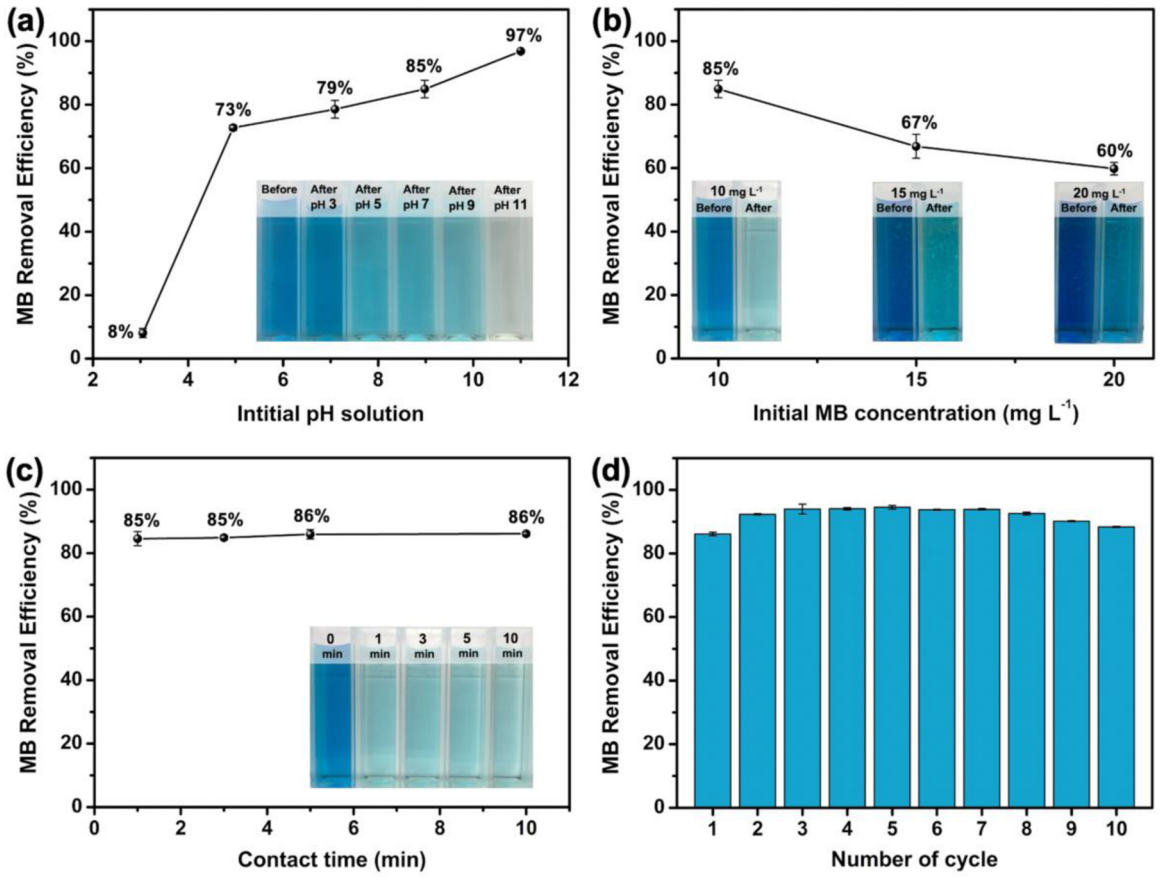

Fig. 8. Effects of (a) initial pH solution, (b) initial MB concentration and (c) contact time on the MB adsorption by $MgFe_2O_4@SiO_2$ NPs. (d) Reusability of $MgFe_2O_4@SiO_2$ NPs for MB adsorption. (insets: digital images of MB solution color before and after adsorption processes).

assumptions such as a homogeneous surface and a single adsorption layer on the adsorbent surface [61,62]. The linear equation form of the Langmuir isotherm can be written as Eq. (3):

$$\frac{C_e}{q_e}=\frac{1}{q_m K_L}+\frac{1}{q_m}C_e \quad (3)$$

where C_e is the dye concentration in solution at equilibrium conditions (mg L^{-1}), q_m is the maximum amount of adsorbed dye on the adsorbent, and K_L is the Langmuir adsorption constant (L mg^{-1}). The values of q_m and K_L can be calculated by using the intercept and slope, respectively, obtained from a straight-line plotting of C_e/q_e *versus* C_e.

The Freundlich adsorption isotherm is contrasts with the Langmuir isotherm *via* parameters such as heterogeneous system and multilayer adsorption [62,63]. The Freundlich isotherm model can be expressed in a linear equation as Eq. (4):

$$\log q_e=\log K_F+\frac{1}{n}\log C_e \quad (4)$$

where K_F and n are the Freundlich empirical constants related to the highest adsorption capacity (L mg^{-1}). Values for 1/n (slope) and $\log K_F$ (intercept) can be obtained from a plot of $\log q_e$ against $\log C_e$.

Fig. *S7* shows the isotherm plots by using the Langmuir and Freundlich models. The parameters of each isotherm model calculated from plots of the adsorption isotherms are also summarized in **Table S3**. The data suggest that the adsorption behavior of MB with $MgFe_2O_4@SiO_2$ NPs could be explained by the Langmuir isotherm model better than the Freundlich isotherm model since the R^2 value of the former plot is 0.996, and that of the latter plot is 0.931. This analysis further indicates that the adsorption behavior of MB occurs *via* monolayer coverage on the $MgFe_2O_4@SiO_2$ surface. However, a quite low value of the maximum adsorption capacity of MB, 4.98 mg g^{-1}, is obtained in this work.

Table S4 shows the comparative removal capacities of MB by different adsorbent types. Several Fe_3O_4-based adsorbents gave various adsorption capacities due to differences in their preparation method. In fact, the adsorbent type is one of the key factors affecting to the adsorption capacity. In terms of practical application, although the $MgFe_2O_4@SiO_2$ nanoadsorbent offers low MB adsorption capacity, the system offers high MB selectivity as well as the capacity for magnetic separation. From this point of view, further studies to increase the adsorption capacity of MB by $MgFe_2O_4@SiO_2$ NPs should be performed, for example, by tuning the thickness of the SiO_2 shell.

3.5. Studies of stability and reusability of $MgFe_2O_4@SiO_2$ NPs for MB adsorption

One of the challenges for adsorbent design is to optimize the performance of the adsorbent in terms of reusability. To address this important issue, we examined the adsorption efficiencies of the $MgFe_2O_4@SiO_2$ nanoadsorbent for ten adsorption-desorption cycles as demonstrated in Fig. 8**d**. These studies found that regeneration by NaOH led to a slight increase from ~86 % to ~94 % in first three cycles. After that, the MB removal efficiencies levelled off at ~94 % from the fourth cycle to the seventh cycle. After the seventh cycle, the adsorption efficiency slightly dropped progressively to ~88 % for the tenth cycle. Overall, the data show that high adsorption efficiencies can be obtained through at least ten regeneration cycles, indicating excellent reusability for MB removal.

With regard to stability, XRD and VSM analyses were performed to investigate the phase and magnetization of the $MgFe_2O_4@SiO_2$ NPs after the adsorption process. **Fig. S8** shows the comparative XRD patterns of the $MgFe_2O_4@SiO_2$ NPs before and after the adsorption

process. No changes of phase occurred with MB treatment. Likewise, the hysteresis loops of the used adsorbent (**Fig. S9**) showed no obvious decline in magnetization compared to the freshly prepared nanoadsorbent. The results of XRD and VSM confirm that the obtained $MgFe_2O_4$@SiO_2 adsorbent system offers high stability for dye removal.

4. Conclusions

Silica-coated magnesium ferrite nanoparticles were used to study the selective adsorption of methylene blue. Characterization by XRD, FT-IR, SEM, TEM, and EDS confirmed the successful synthesis of the $MgFe_2O_4$@SiO_2 NPs. As expected given the increase in nonmagnetic mass, the saturation magnetization of the as-synthesized $MgFe_2O_4$@SiO_2 NPs was less than that of the pristine $MgFe_2O_4$ NPs. Importantly, separation of the nanoadsorbent from the treated solution by an external permanent magnet could be achieved within three minutes. For selective adsorption studies, the results showed a high selectivity for MB adsorption in several dye systems, including single-component dyes, mixtures of two dyes, and mixtures of three dyes. The competitive adsorption of representative dyes was rationalized on the basis of the following: (1) characteristics of the dyes (*i.e.*, molecular charge and size), (2) surface charge of the nanoadsorbent, (3) adsorption conditions, and (4) interactions between nanoadsorbent-adsorbate and adsorbate-adsorbate molecules. Optimized conditions for high removal efficiency of MB by the $MgFe_2O_4$@SiO_2 nanoadsorbent was obtained by using an initial MB concentration of 10 mg L^{-1} at pH ~9 within a few minutes. The adsorption of MB by the $MgFe_2O_4$@SiO_2 NPs followed a Langmuir isotherm model with a maximum adsorption capacity of ~5 mg g^{-1}. After ten adsorption-desorption cycles, high removal efficiencies and stability of the nanoadsorbent system were observed, indicating excellent reusability of the nanoadsorbent. Although the $MgFe_2O_4$@SiO_2 NPs provided a relatively low value for MB adsorption capacity in these initial studies, several attractive characteristics of the nanoadsorbent were observed: (1) facile magnetic separation, (2) good reusability and stability, (3) a rapid adsorption process, and (4) excellent MB selectivity. Collectively, our studies demonstrate that the $MgFe_2O_4$@SiO_2 NPs are useful materials for the adsorption and separation of MB.

CRediT authorship contribution statement

Supawitch Hoijang: Conceptualization, Investigation, Methodology, Writing - original draft. **Sunanta Wangkarn:** Writing - review & editing. **Pimchanok Ieamviteevanich:** Investigation. **Supree Pinitsoontorn:** Investigation, Resources. **Supon Ananta:** Writing - review & editing. **T. Randall Lee:** Writing - review & editing. **Laongnuan Srisombat:** Conceptualization, Methodology, Resources, Writing - original draft, Supervision, Funding acquisition.

Declaration of Competing Interest

The authors declare that they have no known competing financial interests or personal relationships that could have appeared to influence the work reported in this paper.

Acknowledgments

This research work was partially supported by Chiang Mai University and the Global Partnership project,Office of National Higher Education Science Research and Innovation Policy Council. Mr. Supawitch Hoijang would like to acknowledge for the Development and Promotion of Science and Technology Talents (DPST) scholarship for supporting his graduate education. Additional support was provided by the Robert A. Welch Foundation (grant no. E-1320) and the Texas Center for Superconductivity at the University of Houston.

Appendix A. Supplementary data

Supplementary material related to this article can be found, in the online version, at doi:https://doi.org/10.1016/j.colsurfa.2020.125483.

References

[1] M. Rafatullah, O. Sulaiman, R. Hashim, A. Ahmad, Adsorption of methylene blue on low-cost adsorbents: a review, J. Hazard. Mater. 117 (2010) 70–80.
[2] K. Tan, M. Vakili, B. Hord, P. Poh, A. Abdullah, B. Salamatinia, Adsorption of dyes by nanomaterials: recent developments and adsorption mechanisms, Sep. Pur. Technol. 150 (2015) 229–242.
[3] F. Ren, Z. Li, W. Ten, X. Liu, Z. Sun, P. Ren, D. Yan, Facile preparation of 3D regenerated cellulose/graphene oxide composite aerogel with high-efficiency adsorption towards methylene blue, J. Colloid Interface Sci. 532 (2018) 58–67.
[4] P. Zhang, I. Lo, D. O'Connor, S. Pehkonen, H. Cheng, D. Hou, High efficiency removal of methylene blue using SDS surface-modified $ZnFe_2O_4$ nanoparticles, J. Colloid Interface Sci. 508 (2017) 39–48.
[5] L. Liu, Y. Lin, Y. Liu, H. Zhu, Q. He, Removal of methylene blue from aqueous solutions by sewage sludge based granular activated carbon: adsorption equilibrium, kinetics, and thermodynamics, J. Chem. Eng. Data 58 (2013) 2248–2253.
[6] S. Ghorai, A. Sarkar, M. Raoufi, A. Panda, H. Schonherr, S. Pal, Enhanced removal of methylene blue and methyl violet dyes from aqueous solution using a nanocomposite of hydrolyzed polyacrylamide grafted xanthan gum and incorporated nanosilica, ACS Appl. Mater. Interfaces 6 (2014) 4766–4777.
[7] X. Hou, J. Feng, Y. Ren, Z. Fan, M. Zhang, Synthesis and adsorption properties of spongelike porous $MnFe_2O_4$, Colloids Surf. A 363 (2010) 1–7.
[8] T. Yao, L. Qiao, K. Du, High tough and highly porous graphene/carbon nanotubes hybrid beads enhanced by carbonized polyacrylonitrile for efficient dyes adsorption, Microporous Mesoporous Mater. 292 (2020) 1–8.
[9] B. Safizade, S. Masoudpanah, M. Hasheminiasari, A. Ghasemi, Photocatalytic activity of $BiFeO_3$/$ZnFe_2O_4$ nanocomposites under visible light irradiation, RSC Adv. 8 (2018) 6988–6995.
[10] G. Fan, J. Tong, F. Li, Visible-light-induced photocatalyst based on cobalt-doped zinc ferrite nanocrystals, Ind. Eng. Chem. Res. 51 (2012) 13639–13647.
[11] N. Singh, S. Jana, G. Singh, R. Dey, Graphene-supported TiO_2: study of promotion of charge carrier in photocatalytic water splitting and methylene blue dye degradation, Adv. Compos. Hybrid Mater. 3 (2020) 127–140.
[12] X. Liu, Q. Shao, Y. Zhang, X. Wang, J. Lin, Y. Gan, M. Dong, Z. Guo, Microwave hydrothermal synthesized ZnIn-layered double hydroxides derived ZnIn-layered double oxides for enhanced methylene blue photodegradation, Colloids Surf. A 592 (2020) 124588.
[13] L. Sun, Q. Shao, Y. Zhang, H. Jiang, S. Ge, S. Luo, J. Lin, J. Zhang, S. Wu, M. Dong, Z. Guo, N self-doped ZnO derived from microwave hydrothermal synthesized zeolitic imidazolate framework-8 toward enhanced photocatalytic degradation of methylene blue, J. Colloid Interface Sci. 565 (2020) 142–155.
[14] J. Kim, C. Yeom, Y. Kim, Electrochemical degradation of organic dyes with a porous gold electrode, Korean J. Chem. Eng. 33 (2016) 1855–1859.
[15] M. Panizza, A. Barbucci, R. Ricotti, G. Cerisola, Electrochemical degradation of methylene blue, Sep. Pur. Technol. 54 (2007) 382–387.
[16] X. Shi, C. Wang, Y. Ma, H. Liu, S. Wu, Q. Shao, Z. He, L. Guo, T. Ding, Z. Guo, Template-free microwave-assisted synthesis of FeTi coordination complex yolk-shell microspheres for superior catalytic removal of arsenic and chemical degradation of methylene blue from polluted water, Powder Technol. 356 (2019) 726–734.
[17] X. Yang, F. You, Y. Zhao, Y. Bai, L. Shao, Confinedly assembling surface nanocoating to manipulate nanofiltration membranes for highly-efficient dye removal, ES Energy Environ. 1 (2018) 106–113.
[18] A. Onur, K. Shanmugam, A. Ng, G. Garnier, W. Batchelor, Cellulose fibre-perlite depth filters with cellulose nanofibre top coating for improved filtration performance, Colloids Surf. A 583 (2019) 123997.
[19] M. Ayad, A. El-Nasr, Adsorption of cationic dye (methylene blue) from water using polyaniline nanotubes base, J. Phy. Chem. C 114 (2010) 14377–14383.
[20] Y. Li, Y. Zhou, W. Nie, L. Song, P. Chen, Highly efficient methylene blue dyes removal from aqueous systems by chitosan coated magnetic mesoporous silica nanoparticles, J. Porous Mater. 22 (2015) 1383–1392.
[21] G. Tang, W. Chen, X. Wan, F. Zhang, J. Xu, Construction of magnetic Fe_3O_4 nanoparticles coupled with flower-like $MoSe_2$ nanosheets for efficient adsorptive removal of methylene blue, Colloids Surf. A 587 (2020) 124291.
[22] X. Xia, X. Xu, C. Lin, Y. Yang, L. Zeng, Y. Zheng, X. Wu, W. Li, L. Xiao, Q. Qian, Q. Chen, Microalgal-immobilized biocomposite scaffold fabricated by fused deposition modeling 3D printing technology for dyes removal, ES Mater. Manuf. 7 (2020) 40–50.
[23] Y. You, K. Qu, Z. Huang, R. Ma, C. Shi, X. Li, D. Liu, M. Dong, Z. Guo, Sodium alginate templated hydroxyapatite/calcium silicate composite adsorbents for efficient dye removal from polluted water, Int. J. Biol. Macromol. 41 (2019) 1035–1043.
[24] G. Tang, F. Zhang, J. Xu, Facile synthesis of novel ultrathin-MoO_3 square nanosheets with excellent adsorptive capacity and photocatalytic performance for efficient treatment of Rhodamine B, Micro Nano Lett. 14 (2019) 416–419.
[25] J. Chen, X. Wang, Y. Huang, S. Lv, X. Cao, J. Yun, D. Cao, Adsorption removal of pollutant dyes in wastewater by nitrogen-doped porous carbons derived from natural leaves, Eng. Sci. 5 (2019) 30–38.
[26] G. Tang, F. Zhang, P. Huo, S. Zulfiqarc, J. Xu, Y. Yan, H. Tang, Constructing novel

visible-light-driven ternary photocatalyst of AgBr nanoparticles decorated 2D/2D heterojunction of g-C_3N_4/BiOBr nanosheets with remarkably enhanced photocatalytic activity for water-treatment, Ceram. Int. 45 (2019) 19197–19205.
[27] L. Ai, M. Li, L. Li, Adsorption of methylene blue from aqueous solution with activated carbon/cobalt ferrite/alginate composite beads: kinetics, isotherms, and thermodynamics, J. Chem. Eng. Data 56 (2011) 3475–3483.
[28] R. Foroutan, R. Mohammadi, B. Ramavandi, Elimination performance of methylene blue, methyl violet, and Nile blue from aqueous media using AC/$CoFe_2O_4$ as a recyclable magnetic composite, Environ. Sci. Pollut. Res. 26 (2019) 19523–19539.
[29] Y. Song, Y. Duan, L. Zhou, Multi-carboxylic magnetic gel from hyperbranched polyglycerol formed by thiol-ene photopolymerization for efficient and selective adsorption of methylene blue and methyl violet dyes, J. Colloid Interface Sci. 529 (2018) 139–149.
[30] J. Fu, Q. Xin, X. Wu, Z. Chen, Y. Yan, S. Liu, M. Wang, Q. Xu, Selective adsorption and separation of organic dyes from aqueous solution on polydopamine microspheres, J. Colloid Interface Sci. 461 (2016) 292–304.
[31] Z. Akbari, M. Ghiaci, F. Nezampour, Encapsulation of vanadium phosphorus oxide into TiO_2 matrix for selective adsorption of methylene blue from aqueous solution, J. Chem. Eng. Data 63 (2018) 3923–3932.
[32] D. Wang, H. Shen, L. Guo, C. Wang, F. Fu, Porous BiOBr/Bi_2MoO_6 heterostructures for highly selective adsorption of methylene blue, ACS Omega 1 (2016) 566–577.
[33] L. Huang, M. He, B. Chen, Q. Cheng, B. Hu, Facile green synthesis of magnetic porous organic polymers for rapid removal and separation of methylene blue, ACS Sustainable Chem. Eng. 5 (2017) 4050–4055.
[34] X. Zhou, M. Xu, L. Wang, X. Liu, The adsorption of methylene blue by an amphiphilic block co-poly(arylene ether nitrile) microsphere-based adsorbent: kinetic, isotherm, thermodynamic and mechanistic studies, Nanomaterials 9 (2019) 1–15.
[35] Y. Zhang, G. Li, J. Liu, T. Wang, X. Wang, B. Liu, Y. Liu, Q. Huo, Z. Chu, Synthesis of hierarchical hollow sodium titanate microspheres and their application for selective removal of organic dyes, J. Colloid Interface Sci. 528 (2018) 109–115.
[36] X. Zhao, D. Wang, C. Xiang, F. Zhang, L. Liu, X. Zhou, H. Zhang, Facile synthesis of boron organic polymers for efficient removal and separation of methylene blue, rhodamine B, and rhodamine 6G, ACS Sustainable Chem. Eng. 6 (2018) 16777–16787.
[37] H. Molavi, A. Shojaei, A. Pourghaderi, Rapid and tunable selective adsorption of dyes using thermally oxidized nanodiamond, J. Colloid Interface Sci. 524 (2018) 52–64.
[38] J. Nonkumwong, S. Ananta, L. Srisombat, Effective removal of lead(II) from wastewater by amine-functionalized magnesium ferrite nanoparticles, RSC Adv. 6 (2016) 47382–47393.
[39] J. Nonkumwong, P. Pakawanit, A. Wipatanawin, P. Jantaratana, S. Ananta, L. Srisombat, Synthesis and cytotoxicity study of magnesium ferrite-gold core-shell nanoparticles, Mater. Sci. Eng. C 61 (2016) 123–132.
[40] C. Aoopngan, J. Nonkumwong, S. Phumying, W. Promjantuek, S. Maensiri, P. Noisa, S. Pinitsoontorn, S. Ananta, L. Srisombat, Amine-functionalized and hydroxyl-functionalized magnesium ferrite nanoparticles for Congo red adsorption, ACS Appl, Nano Mater. 2 (2019) 5329–5341.
[41] S. Hoijang, J. Nonkumwong, B. Singhana, S. Wangkarn, S. Ananta, L. Srisombat, Adsorption of 2,4-Dichlorophenoxyacetic acid by magnesium ferrite magnetic nanoparticles modified with amine functional groups, Chiang Mai J. Sci. 47 (2020) 137–146.
[42] Y. Dai, J. Zou, D. Liu, L. Niu, L. Zhou, Y. Zhou, X. Zhang, Preparation of Congo red functionalized Fe_3O_4@SiO_2 nanoparticle and its application for the removal of methylene blue, Colloids Surf. A 550 (2018) 90–98.
[43] J. Zou, Y. Dai, D. Liu, S. Wang, L. Zhou, Y. Zhou, Synthesis of carboxyl-functionalized magnetic nanoparticle for the removal of methylene, Colloids Surf. A 572 (2019) 58–66.
[44] X. Tan, L. Lu, L. Wang, J. Zhang, Facile synthesis of bimodal mesoporous Fe_3O_4@SiO_2 composite for efficient removal of methylene blue, Euro. Inorg. Chem. 18 (2015) 2928–2933.
[45] H. Jung, D. Moon, J. Lee, Quantitative analysis and efficient surface modification of silica nanoparticles, J. Nanomater. 2012 (2012) 1–8.
[46] Y. Xu, J. Jin, X. Li, Y. Han, H. Meng, T. Wang, X. Zhang, Fabrication of hybrid magnetic HKUST-1 and its highly efficient adsorption performance for Congo red dye, RSC Adv. 5 (2015) 19199–19202.
[47] M. Obaidullah, N. Bahadur, T. Furusawa, M. Sato, H. Sakuma, N. Suzuki, Microwave assisted rapid synthesis of Fe_2O_3@SiO_2 core-shell nanocomposite for the persistence of magnetic property at high temperature, Colloids Surf. A 572 (2019) 138–146.
[48] I. Rahman, V. Padavettan, Synthesis of silica nanoparticles by sol-gel: size-dependent properties, surface modification, and applications in silica-polymer nanocomposites-a review, J. Nanomate. 2012 (2012) 1–15.
[49] P. Post, L. Wurlitzer, W. Maus-Friedrichs, A. Weber, Characterization and applications of nanoparticles modified in-flight with silica or silica-organic coatings, Nanomaterials 7 (2018) 1–19.
[50] R. Wo, Q. Li, C. Zhu, Y. Zhang, G. Qiao, K. Lei, P. Du, W. Jiang, Preparation and characterization of functionalized metal-organic frameworks with core/shell magnetic particles (Fe_3O_4@SiO_2@MOFs) for removal of Congo red and methylene blue from water solution, J. Chem. Eng. Data 64 (2019) 2455–2463.
[51] P. Xie, Y. Li, Q. Hou, K. Sui, C. Liu, X. Fu, J. Zhang, V. Murugadoss, J. Fan, Y. Wang, R. Fan, Z. Guo, Tunneling-induced negative permittivity in Ni/MnO nanocomposites by a bio-gel derived strategy, J. Mater. Chem. C 8 (2020) 3029–3039.
[52] H. Wang, C. Zhang, B. Zhou, Z. Zhang, J. Shen, A. Du, Ultra-black carbon@silica core-shell aerogels with controllable electrical conductivities, Adv. Compos. Hybrid Mater. 2 (2019) 743–752.
[53] J. Fu, J. Zhu, Z. Wang, Y. Wang, S. Wang, R. Yan, Q. Xu, Highly-efficient and selective adsorption of anionic dyes onto hollow polymer microcapsules having a high surface-density of amino groups: isotherms, kinetics, thermodynamics and mechanism, J. Colloid Interface Sci. 542 (2019) 123–135.
[54] R. Dutta, S. Bhat, Association of neutral red with micelles and its effect on the pKa, Can. J. Chem. 71 (1993) 1785–1791.
[55] X. Zhuang, Y. Wan, C. Feng, Y. Shen, D. Zhao, Highly efficient adsorption of bulky dye molecules in wastewater on ordered mesoporous carbons, Chem. Mater. 21 (2009) 706–716.
[56] S. Huo, X. Yan, Metal-organic framework MIL-100(Fe) for the adsorption of malachite green from aqueous solution, J. Mater. Chem. 22 (2012) 7449–7455.
[57] P. Trujillo, T. Gonzalez, J. Brito, A. Briceno, Surface recognition directed selective removal of dyes from aqueous solution on hydrophilic functionalized petroleum coke sorbents, A supramolecular perspective Ind. Eng. Chem. Res. 58 (2019) 14761–14774.
[58] L. Yang, Y. Zhang, X. Liu, X. Jiang, Z. Zhang, T. Zhang, L. Zhang, The investigation of synergistic and competitive interaction between dye Congo red and methyl blue on magnetic $MnFe_2O_4$, Chem. Eng. J. 246 (2014) 88–96.
[59] L. Zeng, L. Xiao, Y. Long, X. Shi, Trichloroacetic acid-modulated synthesis of polyoxometalate@UiO-66 for selective adsorption of cationic dyes, J. Colloid Interface Sci. 516 (2018) 274–283.
[60] Y. Duan, Y. Song, L. Zhou, Facile synthesis of polyamidoamine dendrimer gel with multiple amine groups as a super adsorbent for highly efficient and selective removal of anionic dyes, J. Colloid Interface Sci. 546 (2019) 351–360.
[61] L. Kong, H. Adidharma, A new adsorption model based on generalized van der Waals partition function for the description of all types of adsorption isotherms, Chem. Eng. J. 375 (2019) 1–8.
[62] Z. Yang, L. Zhu, L. Chen, Selective adsorption and separation of dyes from aqueous solution by core-shell structured NH_2-functionalized UiO-66 magnetic composites, J. Colloid Interface Sci. 539 (2019) 76–86.
[63] Y. Liu, Y. Kang, B. Mu, A. Wang, Attapulgite/bentonite interactions for methylene blue adsorption characteristics from aqueous solution, Chem. Eng. J. 237 (2014) 403–410.